HHS Public Access

Author manuscript

Gastroenterology. Author manuscript; available in PMC 2022 July 01.

Published in final edited form as:

Gastroenterology. 2021 July ; 161(1): 271–286.e11. doi:10.1053/j.gastro.2021.03.048.

Intestinal Sulfation is Essential to Protect Against Colitis and Colonic Carcinogenesis

Pengfei Xu[1], **Yue Xi**[1,2], **Junjie Zhu**[1], **Min Zhang**[1], **Zigmund Luka**[3], **Donna B. Stolz**[4], **Xinran Cai**[1], **Yang Xie**[1], **Meishu Xu**[1], **Songrong Ren**[1], **Zhiying Huang**[2], **Da Yang**[1], **John D. York**[3], **Xiaochao Ma**[1], **Wen Xie**[1,5,*]

[1]Center for Pharmacogenetics and Department of Pharmaceutical Sciences, University of Pittsburgh, Pittsburgh, Pennsylvania

[2]School of Pharmaceutical Sciences, Sun Yat-sen University, Guangzhou, China

[3]Department of Biochemistry, Vanderbilt University, Nashville, Tennessee

[4]Departments of Cell Biology, University of Pittsburgh, Pittsburgh, Pennsylvania

[5]Department of Pharmacology & Chemical Biology, University of Pittsburgh, Pittsburgh, Pennsylvania

Abstract

Background & Aims: Sulfation is a conjugation reaction essential for numerous biochemical and cellular functions in mammals. The 3'-phosphoadenosine 5'-phosphosulfate (PAPS) synthase 2 (PAPSS2) is the key enzyme to generate PAPS, which is the universal sulfonate donor for all sulfation reactions. The goal of this study is to determine whether and how PAPSS2 plays a role in colitis and colonic carcinogenesis.

Methods: Tissue arrays of human colon cancer specimens, gene expression data, and clinical features of cancer patients were analyzed. Intestinal-specific *Papss2* knockout mice (*Papss2*$^{\Delta IE}$) were created and subjected to dextran sodium sulfate (DSS)-induced colitis, and colonic carcinogenesis induced by combined treatment of azoxymethane (AOM) and DSS, or AOM alone.

Results: The expression of PAPSS2 is decreased in the colon cancers of mice and humans. The lower expression of PAPSS2 in colon cancer patients is correlated with worse survival. *Papss2*$^{\Delta IE}$ mice showed heightened sensitivity to colitis and colon cancer by damaging the intestinal mucosal barrier, increasing intestinal permeability and bacteria infiltration, and worsening the intestinal tumor microenvironment. Mechanistically, the *Papss2*$^{\Delta IE}$ mice exhibited reduced intestinal

[*]**Corresponding author:** Department of Pharmaceutical Sciences, University of Pittsburgh, Pittsburgh, PA 15261, wex6@pitt.edu.
Author contributions: W. X. conceived and mentored this research. W.X. and P.X. designed the study. P.X., Y.X., J.Z., M. Z., Z. L., X.C., and Y.X., performed the experiments and analyzed the data. D.B.S., M.X., S.R., Z.H., D.Y., J.D.Y, and X.M. gave technical support and conceptual advice. W.X. and P.X. wrote the manuscript. All authors edited the manuscript and approved the final manuscript.

Disclosures: None.

sulfomucin content. Metabolomic analyses revealed the accumulation of bile acids including the farnesoid X receptor (FXR) antagonist bile acid tauro-β-muricholic acid (T-β-MCA), and deficiency in the formation of bile acid-sulfates in the colon of *Papss2*$^{\Delta IE}$ mice.

Conclusions: We have uncovered an important role of PAPSS2-mediated sulfation in colitis and colonic carcinogenesis. Intestinal sulfation may represent a potential diagnostic marker, and PAPSS2 may serve as a potential therapeutic target for inflammatory bowel disease and colon cancer.

Graphical Abstract

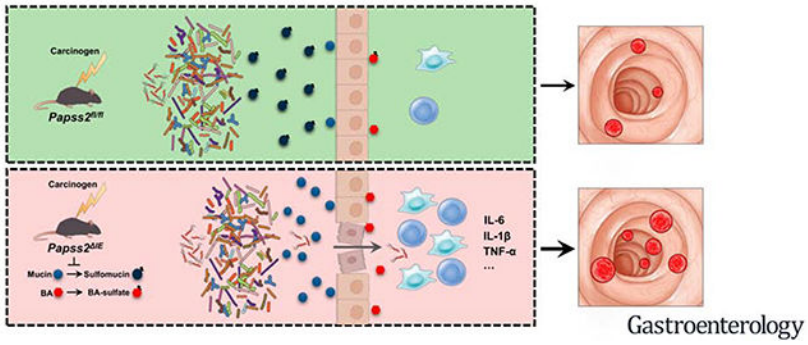

Keywords

Colon cancer; Colitis; PAPSS2; Sulfation; Sulfomucin

Introduction

Colorectal cancer (CRC) is the third most common cancer and the third leading cause of cancer-associated death over the past 30 years [1]. The estimated numbers of new cases and deaths from CRC are 147,950 and 53,200, respectively, in the United States in 2020 according to the American Cancer Society statistics [2]. CRC typically affects older adults; it often begins as polyps (adenoma) inside the bowel wall, which over time can become cancerous. Early detection and intervention are key to ensure a favorable prognosis of CRC.

The etiology and progression of CRC involve both genetic and environmental factors. Genetic factors include familial adenomatous polyposis (FAP), Lynch syndrome, and certain genetic mutations, such as those of the *MLH1*, *MSH2*, *MSH6*, *APC*, *PMS2*, *MUTYH*, *KRAS*, and *TP53* genes [3, 4]. Inflammation associated with inflammatory bowel disease (IBD) such as Crohn's disease (CD) or ulcerative colitis (UC) is one of the most important risk factors for CRC [5]. Indeed, the widely used azoxymethane (AOM)/dextran sodium sulfate (DSS) mouse model of colon cancer is based on tumor initiation by the carcinogen AOM and tumor promotion by DSS-induced colitis [6]. Additional environmental factors for CRC include being overweight, diabetes, and lifestyle factors, such as smoking, alcohol intake, low-fiber and high-fat diet, and lack of physical activity [7]. Although great strides have been made to understand the pathogenesis of CRC, more mechanistic studies are urgently needed in order to identify biomarkers for early detections, or to develop novel therapeutics.

Sulfotransferase (SULT)-mediated sulfation is an essential conjugation reaction. The substrates of sulfation include endogenous and exogenous chemicals, as well as protein peptides [8]. SULTs catalyze the transfer of a sulfonate group from the universal sulfate donor 3′-phosphoadenosine-5′-phosphosulfate (PAPS) to a nucleophilic group of their substrates to generate hydrophilic products. In mammals, PAPS is generated from adenosine trisphosphate (ATP) and inorganic sulfate (SO_4^{2-}), in which the PAPS synthase 2 (PAPSS2) is the key enzyme to catalyze the formation of PAPS [9, 10]. The expression of PAPSS2 is enriched in the endocrine tissues, lung, colon, small intestine, and liver [9]. Patients carrying homozygous loss of function *PAPSS2* mutations exhibit skeletal dysplasia [11, 12]. *PAPSS2* deficiency mutations have also been reported in a young female patient with premature pubarche, hyperandrogenic anovulation as a result of impaired dehydroepiandrosterone sulfation and androgen excess [13, 14]. Decreased intestinal sulfation has been observed in patients with gastrointestinal diseases including IBD, but without mechanistic insight [15–17]. However, whether and how PAPSS2 or sulfation play a role in colitis and colon cancer have not been reported.

In this study, we uncovered an essential function of PAPSS2 in colitis and colonic carcinogenesis. Intestinal ablation of *Papss2* sensitized mice to colitis and colon cancer by compromising the mucosal barrier function as the result of decreased formation of sulfomucin. In humans, the lower expression of PAPSS2 was correlated with worse survival in colon cancer patients.

Materials and Methods

Experimental Animal Studies

Wild-type C57BL/6J and villin-cre mice (B6.Cg-Tg(Vil1-cre)997Gum/J, 004586) were obtained from Jackson Laboratory (Bar Harbor, ME). *Papss2*$^{fl/fl}$ mice, in the C57BL/6 genetic background, were custom-made through embryonic stem cell gene targeting by Ingenious Targeting Laboratory (Ronkonkoma, NY). *Papss2*$^{fl/fl}$ mice were crossed with villin-cre mice to produce intestine-specific *Papss2* null mice (*Papss2*$^{\Delta IE}$). Mice were used in accordance with the University of Pittsburgh Institutional Animal Care and Use Committee. AOM was purchased from Sigma-Aldrich (St. Louis, MO) and colitis grade DSS was from MP Biochemicals (Solon, OH). In DSS-induced colitis model, 8–10 weeks old male *Papss2*$^{fl/fl}$ and *Papss2*$^{\Delta IE}$ mice were treated with 3% DSS (w/v) in drinking water for 6 days. For the AOM/DSS induced colon cancer model, 8-week-old mice were intraperitoneally injected with AOM (10 mg/kg body weight) and followed by two 7-day cycles 2% DSS in drinking water for 16 weeks. For the AOM alone induced colon cancer model, 8-week-old male mice were intraperitoneally injected with AOM (10 mg/kg body weight) once a week for 6 weeks and waited for another 5 months to induce spontaneous colonic carcinogenesis [4]. Mice were killed by CO_2 asphyxiation, then serum samples, colons, and ileums were collected. To test the bile acids content, tissues and serum were collected from mice fasted for 4 h. For BrdU staining, mice were given a single intraperitoneal injection of 60 mg/kg bodyweight BrdU and sacrificed 2 h later.

Analysis of Human Patient Datasets and Human Cohort

Gene expression data and clinical features of cancer patients were downloaded from The Cancer Genome Atlas (TCGA) and Gene Expression Omnibus (GEO) (GSE4107) databases. Human normal and colon tumor tissue array were purchased from US Biomax (Derwood, MD) and used for H&E and immunohistochemical (IHC) staining. Gene expression data and correlation analysis in colonic mucosal biopsies from human colitis patients were obtained from GEO datasets GSE16879 and GSE11223.

Macroscopic and Histological Analysis, Transmission Electron Microscopy and Scanning Electron Microscopy, Biochemical Analysis and Bile Acids Measurement, Assessment of Colitis Severity, Assessment of Intestinal Permeability, Immunostaining and Fluorescence in Situ Hybridization (FISH), Colony Forming Units (CFU) Measurement, Isolation and Culture of Mouse Enteroids, Quantitative Real-Time PCR, Western Blot Analysis, and Statistical Analysis

See Supplementary Methods for details. Information on antibodies and primer sequences is provided in Supplementary Tables 1 and 2.

Results

The Expression of PAPSS2 Decreases in Human and Mouse Colon Cancers

Our analysis of The TCGA database revealed that the *PAPSS2* gene expression was decreased in 14 out of 23 cancer types, including colon cancer (Figure 1A). A decreased expression of *PAPSS2* was also observed in cohort [18] of normal-appearing colonic mucosa of early-onset CRC patients compared to the healthy controls (Figure 1B). The decreased expression of PAPSS2 in human colon cancer was validated by IHC analysis of a colon cancer tissue array including 71 CRC tumors (Figure 1C). Consistent with the human results, the mRNA (Figure 1D) and protein (Figure 1E) expression of Papss2 was decreased in mouse colon cancer induced by AOM/DSS shown by real-time PCR and IHC, respectively. These results suggested that PAPSS2 may play a role in colonic carcinogenesis.

Intestinal Ablation of Papss2 Sensitizes Mice to Colitis

To investigate the intestinal functions of *Papss2* in vivo, we generated intestinal specific *Papss2* knockout (*Papss2*$^{\Delta IE}$) mice by crossbreeding the floxed *Papss2*$^{fl/fl}$ mice with the villin-cre mice. The *Papss2*$^{fl/fl}$ mice were generated by homologous recombination in embryonic stem cells to flox exons 3–6 of the mouse *Papss2* gene as outlined in Figure 2A. The *Papss2*$^{fl/fl}$ and *Papss2*$^{\Delta IE}$ mice were genotyped by PCR (Supplementary Figure 1A). The efficiency of *Papss2* mRNA knockout in the small intestine, colon, and colonic epithelium cells, but not in the liver of *Papss2*$^{\Delta IE}$ mice was confirmed by real-time PCR (Supplementary Figure 1B). The protein knockout of intestinal Papss2 was verified by Western blotting (Supplementary Figure 1C). IHC results showed the endogenous intestinal Papss2 was abundantly expressed in the villi, but this expression was largely abolished in the *Papss2*$^{\Delta IE}$ mice (Supplementary Figure 1D). Consistent with the key role of Papss2 in generating the universal sulfate donor, the PAPS/PAP content was reduced by more than half in colonic epithelium cells harvested from the *Papss2*$^{\Delta IE}$ mice (Figure 2B). Tyrosine

sulfation is the signature of protein sulfation. The total sulfotyrosine level in the colonic epithelium of *Papss2*$^{\Delta IE}$ mice was substantially reduced as shown by immunofluorescence (Figure 2C) or Western blotting (Supplementary Figure 1E) using an anti-sulfotyrosine antibody. The intestinal expression of the *Papss1* isoform was not affected in the *Papss2*$^{\Delta IE}$ mice (Supplementary Figure 2A), and unchallenged *Papss2*$^{\Delta IE}$ mice were healthy and fertile without noticeable phenotypes (Supplementary Figure 2B–2H).

Colitis, such as those associated with IBD, is a major risk factor for colon cancer. Our bioinformatic analysis of the GEO dataset showed that the *PAPSS2* mRNA expression was downregulated in IBD colon biopsies from active inflamed UC and CD patients compared to non-IBD colon biopsies (Figure 2D). The downregulation of *PAPSS2* in IBD patients was accompanied by decreased expression of tight junction proteins, including occludin (*OCLN*) and zonula occludens-1 (*ZO-1*), and increased expression of inflammatory marker genes, such as *IL-6*, *IL-1β*, and *TNFα*, monocytes/macrophages markers (*CD68*, *F4/80*, and *MCP1*), the leukocyte antigen (*CD45*), and the natural T regulatory cell specific marker (*FOXP3*) (Figure 2D).

Knowing the expression of PAPSS2 was decreased in human IBD and the AOM/DSS mouse model of colon cancer, we wanted to determine whether intestinal ablation of *Papss2* sensitizes mice to colitis. In this experiment, male *Papss2*$^{\Delta IE}$ mice and their male *Papss2*$^{fl/fl}$ littermates were treated with 3% DSS in drinking water for 6 days before colon tissue harvesting. Compared to DSS-treated *Papss2*$^{fl/fl}$ controls, DSS-treated *Papss2*$^{\Delta IE}$ mice showed exacerbated colitis, including increased weight loss (Figures 2E), increased disease activity index (Figure 2F), decreased colon weight (Figure 2G) and colon length (Figure 2H), and increased histological mucosal damage (Figure 2I). The organ injury was colon specific, because the small intestine length and weight, spleen weight, and liver weight were not different between the two genotypes (Supplementary Figure 3A–3E). The exacerbated colitis in DSS-treated *Papss2*$^{\Delta IE}$ mice was also manifested by increased inflammation, as evidenced by increased colon and/or ileum mRNA (Figure 2J) and protein (Figure 2K) expression of inflammation and macrophage markers, as well as increased serum levels of inflammatory cytokines (Figure 2L).

Intestinal Ablation of Papss2 Sensitizes Mice to Colon Cancer

We went on to determine whether intestinal ablation of *Papss2* sensitizes mice to colon cancer by using the AOM/DSS model. In the classic AOM/DSS model with a single injection of AOM (10 mg/kg) followed by three 7-day cycles of 2.5% DSS for 10 weeks [19], the *Papss2*$^{\Delta IE}$ mice failed to survive the regimen due to their heightened sensitivity (data not shown). We then reduced DSS to 2% and two 7-day cycles for a total of 16 weeks as outlined in Supplementary Figure 4A and used by others [6]. In this revised regimen, male *Papss2*$^{\Delta IE}$ mice exhibited exacerbated colonic carcinogenesis, as evidenced by the gross appearance of the colon tissues (Figure 3A), increased total tumor area (Figure 3B), tumor numbers (Figure 3C), and the number of large tumors (diameter > 2 mm) (Figure 3D), as well as decreased colon length (Figure 3E). At the histological level, *Papss2*$^{\Delta IE}$ tumors showed increased BrdU labeling and immunostaining (Figure 3F) and Ki67 immunostaining (Figure 3G). The body weight of *Papss2*$^{\Delta IE}$ mice was lower during the AOM/DSS treatment

(Figure 3H), but the percentages of fat and lean mass were not different between *Papss2*$^{fl/fl}$ and *Papss2*$^{\Delta IE}$ mice at sacrificing (Supplementary Figure 4B). Although the survival curve had no significant difference (Supplementary Figure 4C), the mortality rate of the *Papss2*$^{\Delta IE}$ mice (31.3%) was more than twice of the *Papss2*$^{fl/fl}$ controls (14.3%) (Figure 3I). Rectal prolapse often presents as the initial clinical symptom of colon cancer [20]. The AOM/DSS-treated *Papss2*$^{\Delta IE}$ mice exhibited rectal prolapse earlier and at a higher incidence (Figure 3J). The exacerbated colonic carcinogenesis in *Papss2*Δ^{IE} mice was accompanied by increased inflammation, as shown by increased colon and/or ileum mRNA (Figure 3K) and protein (Figure 3L) expression of inflammation and macrophage markers, as well as increased serum levels of inflammatory cytokines (Figure 3M). WT female mice were reported to be less sensitive to AOM/DSS induced colon cancer [21], but we observed a similar pattern of increased colonic carcinogenesis and inflammation in female *Papss2*$^{\Delta IE}$ mice subjected to the same regimen of AOM/DSS (Supplementary Figure 5A–5D), although the effects tended to be less dramatic than their male counterparts.

To determine whether intestinal ablation of *Papss2* sensitizes mice to colon cancer in the absence of colitis promotion, we subjected mice to a standard 6-round AOM administration regimen of colonic carcinogenesis as reported [4]. In this AOM alone model, the male *Papss2*$^{\Delta IE}$ mice exhibited aggravated colonic carcinogenesis, as evidenced by increased tumor incidence (Figure 3N), total tumor area (Figure 3O), as well as decreased colon length (Figure 3P). At the histological level, *Papss2*$^{\Delta IE}$ tumors showed substantially increased Ki67 immunostaining (Figure 3Q).

Intestinal Deficiency of Papss2 Compromises Mucin Sulfation and Gut Barrier Upon Colitis Challenge

Sulfonated carbohydrates represent an abundant component of mucins, which are the major macromolecular component of gastrointestinal mucus and the mucosal glycocalyx. The colonic epithelium is protected by a mucus gel layer composed predominantly of acid mucins synthesized and secreted by the goblet cells [22]. Acid mucins are classified into sulfated (sulfomucin) and non-sulfated (sialomucin) subtypes [23]. Colonic sections were stained with high iron diamine-alcian blue (HID-AB) and periodic acid-Schiff-AB (PAS-AB) to detect sulfomucin and neutral mucin, respectively [24]. The staining of sulfomucin was markedly reduced in untreated (Figure 4A) and DSS-treated (Figure 4B) *Papss2*$^{\Delta IE}$ mice compared to their *Papss2*$^{fl/fl}$ counterparts. In contrast, the levels of neutral mucin were not different between these two genotypes (Supplementary Figure 6A and 6B). Since the intestinal sulfomucin content is essential for gut barrier function [15], we used oral gavage of FITC-dextran [25] to determine whether intestinal deficiency of *Papss2* compromised the gut barrier. The serum levels of FITC-dextran were increased in untreated and DSS-treated *Papss2*$^{\Delta IE}$ mice, and more *in situ* fluorescence signals were observed in the colon sections of DSS-treated *Papss2*$^{\Delta IE}$ mice (Figure 4C), suggesting that the *Papss2*$^{\Delta IE}$ mice had increased intestinal permeability. The structural damage to the gut barrier of DSS-treated *Papss2*$^{\Delta IE}$ mice was further supported by the decreased expression of the tight junction proteins OCLN and ZO-1 as shown by Western blotting (Figure 4D) and immunofluorescence (Figure 4E), increased serum level of endotoxin (Figure 4F), as well as the electron microscopic (EM) analysis. Transmission EM (TEM) showed compromised structural integrity of the tight

junction in DSS-treated *Papss2*$^{\Delta IE}$ mice (Figure 4G, left). Scanning EM (SEM) revealed rough surfaces of the colonic microvilli in DSS-treated *Papss2*$^{\Delta IE}$ mice, in contrast to the smooth-looking surface of microvilli in their *Papss2*$^{fl/fl}$ counterparts (Figure 4G, right). In the absence of DSS challenge, the expression of tight junction proteins was not affected by *Papss2* ablation (Supplementary Figure 7A and 7B), and the enteroid formation was not different between these two genotypes either (Supplementary Figure 7C).

At the functional levels, FISH (Figure 4H) and CFU assay (Figure 4I) showed DSS-treated *Papss2*$^{\Delta IE}$ mice had increased bacterial infiltration into the epithelium and bacterial translocation. The colonic immunostaining and activity of MPO, a marker of neutrophil and monocyte infiltrations, were increased in DSS-treated *Papss2*$^{\Delta IE}$ mice (Figure 4J), and so was the immunostaining of Cd68, a macrophage marker (Figure 4K). Macrophages can be divided into M1 (pro-inflammatory) and M2 (anti-inflammatory) subtypes [26]. The aggravated colitis in *Papss2*$^{\Delta IE}$ mice was accompanied by increased mRNA expression (Figure 4L) and immunostaining (Figure 4M) of M1, but not M2 markers.

Intestinal Ablation of Papss2 Impairs Intestinal Barrier Function and Worsens Tumor Microenvironment in Tumor-Bearing Mice

A decreased sulfomucin content was also observed in the colon of AOM/DSS induced tumor-bearing *Papss2*$^{\Delta IE}$ mice. HID-AB staining showed a lower sulfomucin content in the epithelium of the non-tumor area of the *Papss2*$^{\Delta IE}$ mice, whereas the intratumor sulfomucin was barely detectable (Figure 5A). In normal conditions, the colonic mucus layer forms a barrier that prevents bacteria from entering the epithelium [27]. As shown in Figure 5B, the thickness of the mucus layer was decreased in both untreated and AOM/DSS-treated *Papss2*$^{\Delta IE}$ mice. Consistent with results from the colitis model, the AOM/DSS-treated *Papss2*$^{\Delta IE}$ mice showed a leaky gut by having a higher serum level of FITC-dextran (Figure 5C), decreased expression of tight junction proteins (Figure 5D and 5E), and increased serum level of endotoxin (Figure 5F). AOM/DSS-treated *Papss2*$^{\Delta IE}$ mice had increased bacterial infiltration into the epithelium and bacterial translocation as shown by FISH (Figure 5G) and CFU assay (Figure 5H). The infiltration of Cd68 positive macrophages (Figure 5I) and expression of M1, but not M2 markers (Figure 5J and 5K) was also elevated in AOM/DSS-treated *Papss2*$^{\Delta IE}$ mice, suggesting a worsened tumor microenvironment.

Increased Colonic Carcinogenesis in Papss2$^{\Delta IE}$ Mice is Accompanied by Disruption of Bile Acid Homeostasis and FXR Signaling

Bile acids play an important role in the pathogenesis of colon cancer [28]. We and others have reported that sulfation is an important metabolic pathway to detoxify and eliminate bile acids, because bile acid sulfates are less toxic than unsulfated bile acids, and they are more water-soluble and readily excreted through the urine and feces [29]. Farnesoid X receptor (FXR) is a bile acid receptor whose activation has been shown to have anti-colon cancer activity [28]. The AOM/DSS-treated *Papss2*$^{\Delta IE}$ mice showed increased levels of bile acids in the serum (Figure 6A) and colon tissues (Figure 6B). But to our surprise, the colonic mRNA expression of FXR target genes, including *Fgf15*, *Shp*, and *Ibabp*, was markedly decreased in AOM/DSS-treated *Papss2*$^{\Delta IE}$ mice (Figure 6C). Bile acid species profiling showed the colon tissue levels of several FXR antagonists, including tauro-alpha-muricholic acid (T-α-

MCA), T-β-MCA, and ursodeoxycholic acid (UDCA), were elevated in AOM/DSS-treated *Papss2*$^{\Delta IE}$ mice, which may have explained the inhibition of FXR activity. Meanwhile, the levels of chenodeoxycholic acid (CDCA) and other MCAs were increased in *Papss2*$^{\Delta IE}$ mice (Figures 6D and E). When the sulfonated bile acid species were analyzed, we found the colon tissue levels deoxycholic acid (DCA)-sulfate, cholic acid (CA)-sulfate, and taurocholic acid (TCA)-sulfate were decreased (Figure 6F), whereas the levels of the parent DCA, CA, and TCA were increased in the *Papss2*$^{\Delta IE}$ mice, in particular upon the AOM/DSS treatment (Figure 6G).

Decreased Expression of PAPSS2 Correlates with Poor Clinical Outcome of Colon Cancer Patients

In understanding the human relevance of decreased expression of PAPSS2 in colon cancer, we found a lower expression of *PAPSS2* was strongly correlated with poorer survival in the TCGA cohorts of colon adenocarcinoma (COAD) and CRC patients (Figure 7A). Analysis of an independent CRC patient cohort (GSE4107) revealed that the colonic mucosa of colon cancer patients showed decreased expression of *PAPSS2* and *OCLN*, but increased expression of inflammatory markers, monocytes/macrophages markers, leukocyte antigen, and natural T regulatory cell marker genes (Figure 7B). Gene Expression Profiling Interactive Analysis (GEPIA) web server [30] analyses of the human COAD patients showed the expression of *PAPSS2* has a strong positive correlation with the expression of *OCLN* (Figure 7C). In human IBD patients, the expression of *PAPSS2* showed inverse correlations with those of *IL-1β*, *IL-6*, and *TNFα*, but a positive correlation with that of *OCLN* (Figure 7D). These results indicated that down-regulation of *PAPSS2* is strongly associated with inflammation, compromised gut barrier, and colonic carcinogenesis. We propose that the intestinal PAPSS2 protects against colitis-associated carcinogenesis by improving mucosal barrier functions and ameliorating inflammatory response through the promotion of mucin and bile acid sulfation as depicted in Figure 7E.

Discussion

In this study, we showed that low expression of PAPSS2 was associated with increased incidence of human colitis and colon cancer. Intestinal ablation of *Papss2* in mice promoted DSS-induced colitis and AOM-induced colonic carcinogenesis in the presence or absence of DSS promotion. PAPSS2 protects against colitis and associated colonic carcinogenesis through intestinal sulfomucin and promotion of bile acid homeostasis via the PAPSS2-PAPS-sulfation axis.

The gastrointestinal epithelial surfaces are covered with a layer of protective mucinous gel composed predominantly of mucins [31]. Sulfonated glycoproteins are the major macromolecular and mucosal glycocalyx, which are the important components of mucins for lubricating and protecting the underlying intestinal epithelium [32]. Mucin 2 (MUC2) is the most abundant mucin in the colonic mucinous layer [33]. *Muc2* knockout mice exhibited spontaneous intestinal tumor formation and increased inflammation as a result of a breached epithelial barrier, increased lymphocyte infiltration and expression of inflammatory cytokine genes [34, 35]. Mucin can be sulfonated, and the *N*-acetylglucosamine 6-*O*-sulfotransferase-2

(GlcNAc6ST-2) is the primary sulfotransferase that catalyzes the sulfation of mucin-like glycoproteins in the colonic epithelial cells. *GlcNAc6ST-2* null mice exhibited accelerated leukocyte and macrophage infiltration to the colonic epithelium by diminishing GlcNAc-6-*O*-sulfation in the DSS colitis model [36]. The sodium sulfate cotransporter 1 (NaS1), also known as SLC13A1, is responsible for the absorption of inorganic sulfate [37]. The *NaS1*-deficient mice showed reduced intestinal sulfomucin content and impaired intestinal barrier function in toxin-induced colitis [15]. Although the *Muc2*-, *GlcNAc6ST-2*, and *NaS1*-deficient mice shared a common phenotype of impaired mucosal barrier and aggravated DSS-induced colitis, a major limitation of these studies is that whole-body knockout mice were used, and these mice often had systemic phenotypes even in the absence of colitis challenge, such as growth retardation in *Muc2* and *NaS1* knockout mice, and inhibition of lymphocyte homing in *GlcNAc6ST-2* null mice. As such, it is unclear whether their intestinal phenotypes were due to intestinal loss of the gene functions, or they were secondary to the systemic phenotypes. Our unchallenged *Papss2*$^{\Delta IE}$ mice were healthy and not different from their *Papss2*$^{fl/fl}$ littermates. The expression of *Muc-2*, *NaS1*, *GlcNAc6ST-2* was not different in the colon of vehicle, DSS, and AOM/DSS treated *Papss2*$^{fl/fl}$ and *Papss2*$^{\Delta IE}$ mice (Supplementary Figure 8). We conclude that the intestinal ablation of *Papss2* was sufficient to compromise the mucosal barrier.

Our results are highly human relevant. Low colonic sulfate and mucin sulfation have been reported in human ulcerative colitis [15]. In the current study, our bioinformatic analysis of the TCGA and GEO datasets showed the mRNA expression of *PAPSS2* was decreased in colitis and colon cancer, which was verified by human colon cancer tissue array. Moreover, we found that decreased expression of PAPSS2 correlates with poor clinical outcomes of colon cancer patients. Besides decreased sulfomucin, intestinal ablation of *Papss2* in mice or decreased expression of PAPSS2 in human colon cancer was associated with decreased expression of tight junction proteins. The mechanism by which deficiency of PAPSS2 suppresses the expression of tight junction proteins remains to be understood. Nevertheless, the decreased expression of tight junction proteins may have also contributed to the compromised gut barrier and increased colonic carcinogenesis in *Papss2*$^{\Delta IE}$ mice and PAPSS2-low expressing patients.

Another interesting finding is the disruption of bile acid homeostasis in the *Papss2*$^{\Delta IE}$ mice. Emerging evidence indicates a strong association between the abundance and species of intestinal bile acids and the development of colitis and colon cancer. Several secondary bile acid species, DCA in particular, influence multiple signaling pathways in enterocytes that can lead to the development of CRC [28, 38]. Sulfation of bile acids is a major pathway for bile acid elimination and detoxification [29]. We found the sulfation of DCA, CA, TCA was decreased, and the levels of parent DCA, CA, TCA were increased in the *Papss2*$^{\Delta IE}$ mice.

An intriguing finding related to bile acids is the accumulation of FXR antagonist bile acids including T-β-MCA, and inhibition of FXR signaling in AOM/DSS-treated *Papss2*$^{\Delta IE}$ mice, which may have also contributed to the increased colonic carcinogenesis. FXR is a bile acid receptor whose activation protects against intestinal tumorigenesis. Loss of FXR sensitized mice to the adenomatous polyposis coli (APC)$^{min/+}$ and chronic colitis mouse models of intestinal tumorigenesis [39, 40]. A more recent report suggested that the antagonistic T-βMCA

induced proliferation and DNA damage in $Lgr5^{+}$ cancer stem cells, leading to CRC progression [41]. The mechanism by which FXR antagonist bile acids were accumulated in AOM/DSS-treated *Papss2*$^{\Delta IE}$ mice remains to be understood.

Besides CRC, decreased expressions of *PAPSS2* were also observed in several other cancer types, including lung adenocarcinoma, lung squamous cell carcinoma, uterine corpus endometrial carcinoma, bladder urothelial carcinoma, kidney renal papillary cell carcinoma, liver hepatocellular carcinoma, breast invasive carcinoma, cholangiocarcinoma, kidney renal clear cell carcinoma, thyroid carcinoma, kidney chromophobe, and pheochromocytoma and paraganglioma. Future studies are necessary to determine whether and how PAPSS2 plays a role in the pathogenesis of other cancer types.

In conclusion, we showed the PAPSS2-PAPS-sulfation axis plays an essential role in colitis and colonic carcinogenesis. We propose that intestinal sulfation may represent a potential diagnostic marker, and PAPSS2 may serve as a potential therapeutic target for IBD and colon cancer.

Supplementary Material

Refer to Web version on PubMed Central for supplementary material.

Acknowledgements

This work was supported in part by National Institutes of Health grant ES030429 (to W.X.). Y.X. is a visiting student from Sun Yat-sen University supported by a Visiting Student Scholarship from the Government of China's China Scholarship Council (File no. 201806380128).

References

1. Bray F, Ferlay J, Soerjomataram I, et al. Global cancer statistics 2018: GLOBOCAN estimates of incidence and mortality worldwide for 36 cancers in 185 countries. CA Cancer J Clin 2018;68:394–424. [PubMed: 30207593]
2. Siegel RL, Miller KD, Jemal A. Cancer statistics, 2020. CA Cancer J Clin 2020;70:7–30. [PubMed: 31912902]
3. Ten Broeke SW, van Bavel TC, Jansen AML, et al. Molecular Background of Colorectal Tumors From Patients With Lynch Syndrome Associated With Germline Variants in PMS2. Gastroenterology 2018;155:844–851. [PubMed: 29758216]
4. Luo Y, Xie C, Brocker CN, et al. Intestinal PPARalpha Protects Against Colon Carcinogenesis via Regulation of Methyltransferases DNMT1 and PRMT6. Gastroenterology 2019;157:744–759 e4. [PubMed: 31154022]
5. Rhodes JM, Campbell BJ. Inflammation and colorectal cancer: IBD-associated and sporadic cancer compared. Trends Mol Med 2002;8:10–6. [PubMed: 11796261]
6. De Robertis M, Massi E, Poeta ML, et al. The AOM/DSS murine model for the study of colon carcinogenesis: From pathways to diagnosis and therapy studies. J Carcinog 2011;10:9. [PubMed: 21483655]
7. Murphy N, Moreno V, Hughes DJ, et al. Lifestyle and dietary environmental factors in colorectal cancer susceptibility. Mol Aspects Med 2019;69:2–9. [PubMed: 31233770]
8. Kauffman FC. Sulfonation in pharmacology and toxicology. Drug Metab Rev 2004;36:823–43. [PubMed: 15554249]
9. Leung AW, Backstrom I, Bally MB. Sulfonation, an underexploited area: from skeletal development to infectious diseases and cancer. Oncotarget 2016;7:55811–55827. [PubMed: 27322429]

10. Mueller JW, Idkowiak J, Gesteira TF, et al. Human DHEA sulfation requires direct interaction between PAPS synthase 2 and DHEA sulfotransferase SULT2A1. J Biol Chem 2018;293:9724–9735. [PubMed: 29743239]
11. Miyake N, Elcioglu NH, Iida A, et al. PAPSS2 mutations cause autosomal recessive brachyolmia. J Med Genet 2012;49:533–8. [PubMed: 22791835]
12. Faiyaz ul Haque M, King LM, Krakow D, et al. Mutations in orthologous genes in human spondyloepimetaphyseal dysplasia and the brachymorphic mouse. Nat Genet 1998;20:157–62. [PubMed: 9771708]
13. Oostdijk W, Idkowiak J, Mueller JW, et al. PAPSS2 deficiency causes androgen excess via impaired DHEA sulfation--in vitro and in vivo studies in a family harboring two novel PAPSS2 mutations. J Clin Endocrinol Metab 2015;100:E672–E680. [PubMed: 25594860]
14. Noordam C, Dhir V, McNelis JC, et al. Inactivating PAPSS2 mutations in a patient with premature pubarche. N Engl J Med 2009;360:2310–8. [PubMed: 19474428]
15. Dawson PA, Huxley S, Gardiner B, et al. Reduced mucin sulfonation and impaired intestinal barrier function in the hyposulfataemic NaS1 null mouse. Gut 2009;58:910–9. [PubMed: 19201772]
16. Corfield AP, Myerscough N, Bradfield N, et al. Colonic mucins in ulcerative colitis: evidence for loss of sulfation. Glycoconj J 1996;13:809–22. [PubMed: 8910008]
17. Raouf AH, Tsai HH, Parker N, et al. Sulphation of colonic and rectal mucin in inflammatory bowel disease: reduced sulphation of rectal mucus in ulcerative colitis. Clin Sci (Lond) 1992;83:623–6. [PubMed: 1335401]
18. Hong Y, Ho KS, Eu KW, et al. A susceptibility gene set for early onset colorectal cancer that integrates diverse signaling pathways: implication for tumorigenesis. Clin Cancer Res 2007;13:1107–14. [PubMed: 17317818]
19. Kim JJ, Shajib MS, Manocha MM, et al. Investigating intestinal inflammation in DSS-induced model of IBD. J Vis Exp 2012;60:e3678.
20. Chen CW, Hsiao CW, Wu CC, et al. Rectal prolapse as initial clinical manifestation of colon cancer. Z Gastroenterol 2008;46:348–50. [PubMed: 18393153]
21. Lee SM, Kim N, Son HJ, et al. The Effect of Sex on the Azoxymethane/Dextran Sulfate Sodium-treated Mice Model of Colon Cancer. J Cancer Prev 2016;21:271–278. [PubMed: 28053962]
22. Martinez CA, Nonose R, Spadari AP, et al. Quantification by computerized morphometry of tissue levels of sulfomucins and sialomucins in diversion colitis in rats. Acta Cir Bras 2010;25:231–40. [PubMed: 20498935]
23. Deplancke B, Gaskins HR. Microbial modulation of innate defense: goblet cells and the intestinal mucus layer. Am J Clin Nutr 2001;73:1131S–1141S. [PubMed: 11393191]
24. Matsuo K, Ota H, Akamatsu T, et al. Histochemistry of the surface mucous gel layer of the human colon. Gut 1997;40:782–9. [PubMed: 9245933]
25. Garbacz WG, Uppal H, Yan J, et al. Chronic Activation of Liver X Receptor Sensitizes Mice to High Cholesterol Diet-Induced Gut Toxicity. Mol Pharmacol 2018;94:1145–1154. [PubMed: 30045953]
26. Li G, Liu D, Kimchi ET, et al. Nanoliposome C6-Ceramide Increases the Anti-tumor Immune Response and Slows Growth of Liver Tumors in Mice. Gastroenterology 2018;154:1024–1036 e9. [PubMed: 29408569]
27. Johansson ME, Gustafsson JK, Holmen-Larsson J, et al. Bacteria penetrate the normally impenetrable inner colon mucus layer in both murine colitis models and patients with ulcerative colitis. Gut 2014;63:281–91. [PubMed: 23426893]
28. Gadaleta RM, Garcia-Irigoyen O, Moschetta A. Bile acids and colon cancer: Is FXR the solution of the conundrum? Mol Aspects Med 2017;56:66–74. [PubMed: 28400119]
29. Alnouti Y Bile Acid sulfation: a pathway of bile acid elimination and detoxification. Toxicol Sci 2009;108:225–46. [PubMed: 19131563]
30. Tang Z, Li C, Kang B, et al. C. Nucleic Acids Res 2017;45:W98–W102.
31. Martens EC, Neumann M, Desai MS. Interactions of commensal and pathogenic microorganisms with the intestinal mucosal barrier. Nat Rev Microbiol 2018;16:457–470. [PubMed: 29904082]

32. Gendler SJ, Spicer AP. Epithelial mucin genes. Annu Rev Physiol 1995;57:607–34. [PubMed: 7778880]
33. McGuckin MA, Linden SK, Sutton P, et al. Mucin dynamics and enteric pathogens. Nat Rev Microbiol 2011;9:265–78. [PubMed: 21407243]
34. Van der Sluis M, De Koning BA, De Bruijn AC, et al. Muc2-deficient mice spontaneously develop colitis, indicating that MUC2 is critical for colonic protection. Gastroenterology 2006;131:117–29. [PubMed: 16831596]
35. Velcich A, Yang W, Heyer J, et al. Colorectal cancer in mice genetically deficient in the mucin Muc2. Science 2002;295:1726–9. [PubMed: 11872843]
36. Tobisawa Y, Imai Y, Fukuda M, et al. Sulfation of colonic mucins by N-acetylglucosamine 6-O-sulfotransferase-2 and its protective function in experimental colitis in mice. J Biol Chem 2010;285:6750–60. [PubMed: 20018871]
37. Lee A, Beck L, Markovich D. The human renal sodium sulfate cotransporter (SLC13A1; hNaSi-1) cDNA and gene: organization, chromosomal localization, and functional characterization. Genomics 2000;70:354–63. [PubMed: 11161786]
38. Jia W, Xie G, Jia W. Bile acid-microbiota crosstalk in gastrointestinal inflammation and carcinogenesis. Nat Rev Gastroenterol Hepatol 2018;15:111–128. [PubMed: 29018272]
39. Modica S, Murzilli S, Salvatore L, et al. Nuclear bile acid receptor FXR protects against intestinal tumorigenesis. Cancer Res 2008;68:9589–94. [PubMed: 19047134]
40. Maran RR, Thomas A, Roth M, et al. Farnesoid X receptor deficiency in mice leads to increased intestinal epithelial cell proliferation and tumor development. J Pharmacol Exp Ther 2009;328:469–77. [PubMed: 18981289]
41. Fu T, Coulter S, Yoshihara E, et al. FXR Regulates Intestinal Cancer Stem Cell Proliferation. Cell 2019;176:1098–1112. [PubMed: 30794774]

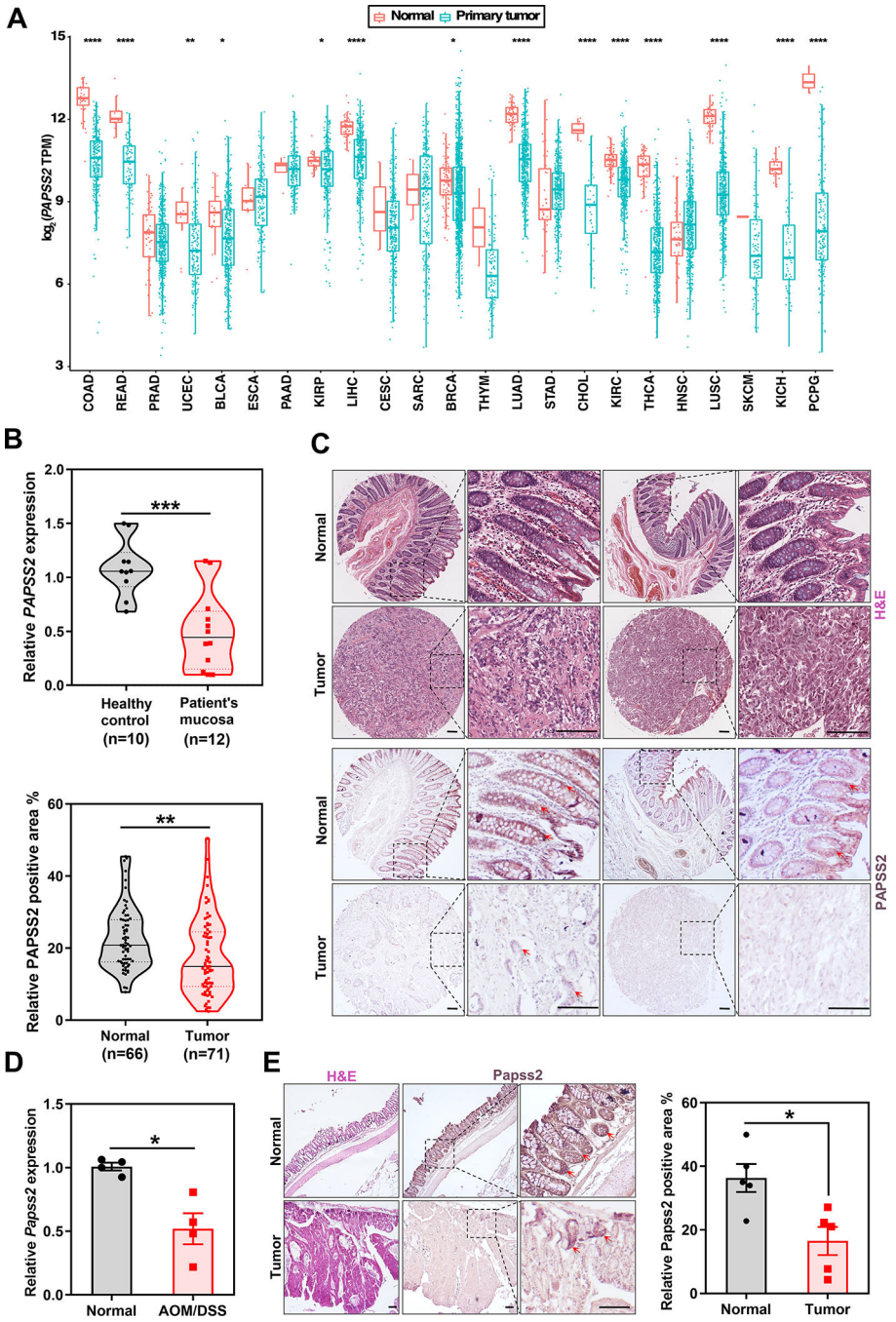

Figure 1. The expression of PAPSS2 is decreased in human and mouse colon cancers.

(A) Analysis of *PAPSS2* gene expression in normal and primary tumors in different TCGA cohorts of cancers. COAD, colon adenocarcinoma; READ, rectum adenocarcinoma; PRAD, prostate adenocarcinoma; UCEC, uterine corpus endometrial carcinoma; BLCA, bladder urothelial carcinoma; ESCA, esophageal carcinoma; PAAD, pancreatic adenocarcinoma; KIRP, kidney renal papillary cell carcinoma; LIHC, liver hepatocellular carcinoma; CESC, cervical squamous cell carcinoma and endocervical adenocarcinoma; SARC, sarcoma; BRCA, breast invasive carcinoma; THYM, thymoma; LUAD, lung adenocarcinoma; STAD,

stomach adenocarcinoma; CHOL, cholangiocarcinoma; KIRC, kidney renal clear cell carcinoma; THCA, thyroid carcinoma; HNSC, head and neck squamous cell carcinoma; LUSC, lung squamous cell carcinoma; SKCM, skin cutaneous melanoma; KICH, kidney chromophobe; PCPG, pheochromocytoma and paraganglioma.
(B) *PAPSS2* gene expression in healthy and colon cancer patient's mucosa (GSE4107).
(C) Representative H&E and IHC staining of PAPSS2 on human normal and colon cancer tissue array. Red arrows indicate positive staining. Shown lower left is the quantifications of PAPSS2 positive area. (D) Relative colonic expression of *Papss2* in AOM/DSS-induced colon cancer model. (E) Representative H&E and IHC staining of Papss2 on AOM/DSS-induced mouse colon tumor and adjacent normal mucosa. Red arrows indicate positive staining. Shown on the right is the quantifications of Papss2 positive area. Scale bars: 100 μm. Data are presented as the mean ± SEM. $*P < .05$, $**P < .01$, $***P < .001$, $****P < .0001$.

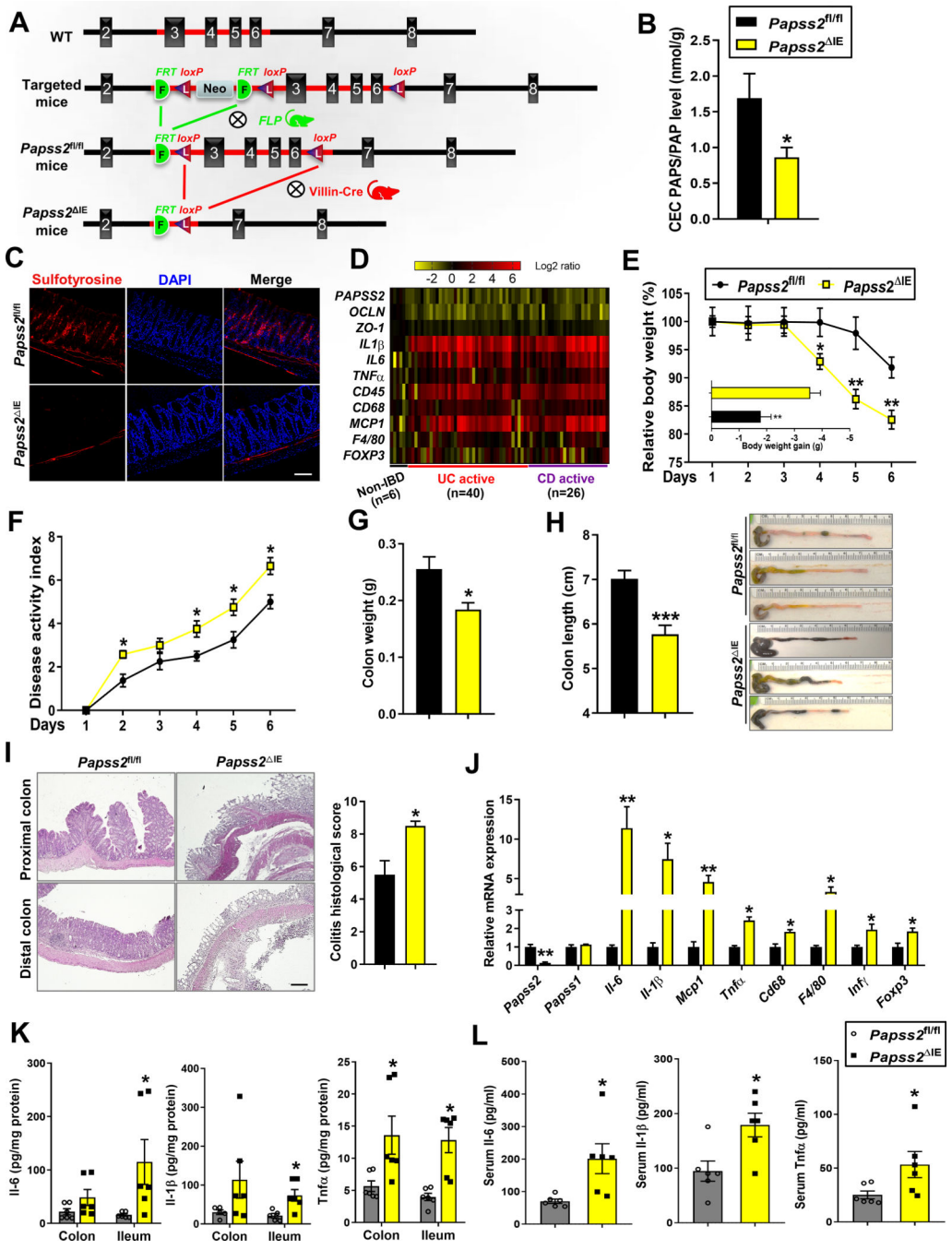

Figure 2. Intestinal ablation of *Papss2* sensitizes mice to colitis.

(A) Schematic representation of the creation of *Papss2*$^{fl/fl}$ and *Papss2*$^{\Delta IE}$ mice. (B) Quantification of PAPS and PAP content in the colonic epithelium cells (CEC) (n=5). (C) Immunofluorescence of sulfotyrosine (Red) in colon sections from untreated *Papss2*$^{fl/fl}$ and *Papss2*$^{\Delta IE}$ mice. (D) Heat map comparing gene expression in mucosal biopsies from non-IBD subjects and actively inflamed mucosa from UC and CD patients (GSE16879). (E-L) Eight-week-old male mice were treated with 3% DSS in drinking water for 6 days. (n=6). (E) Relative body weight and body weight gain (insert). (F) Disease activity index. (G)

Colon weight. (H) Colon length and representative appearance of colons (right). (I) H&E staining of distal and proximal colon sections. Shown on the right is the colitis histological scores. (J) Relative inflammatory cytokine mRNA levels in the colon were measured by real-time PCR. (K and L) Colon and ileum (K) and serum (L) levels of Il-6, Il-1β, and Tnfα were measured by ELISA. Scale bars: 100 μm. Data are presented as the mean ± SEM. *$P < .05$, **$P < .01$, ***$P < .001$.

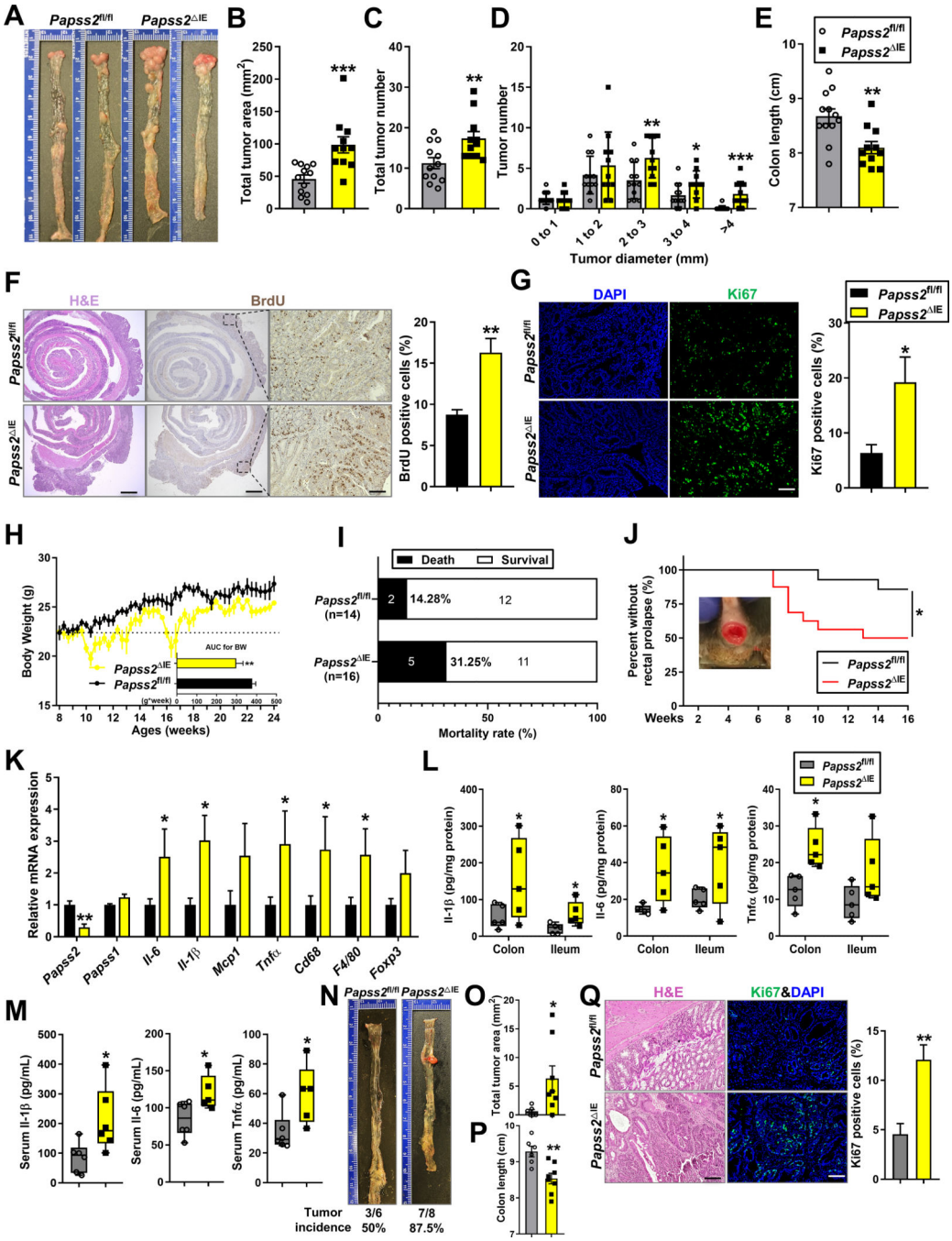

Figure 3. Intestinal ablation of *Papss2* sensitizes mice to colon cancer.

(A-M) Eight-week-old male mice were subjected to the 16-week AOM/DSS model of colon cancer. n=14–16. (A) Representative gross appearance of the colons. (B) Total tumor area. (C) Total tumor number. (D) Tumor size distribution. (E) Colon length. (F) Representative H&E (left) and BrdU immunostaining (middle and right) of colon sections and BrdU labeling index (n=5). Left and middle scale bars: 1 mm, right scale bars: 100 μm. (G) Representative immunofluorescence of Ki67 (green) in colon sections and Ki67 positive index (right) (n=5). Scale bars: 100 μm. (H) Body weight curve and body weight AUC

(insert). (I) Prevalence of mortality. (J) Prevalence of rectal prolapse, and representative appearance of rectal prolapse (insert). (K) Relative colonic inflammatory cytokine mRNA levels (n=5). (L) Colonic and ileal levels of Il-1β, Il-6, and Tnfα. (M) Serum levels of Il-1β, Il-6, and Tnfα. (N-Q) Eight-week-old male mice were subjected to the AOM alone model of colon cancer for 6.5 months. n=6–8. (N) Representative gross appearance of the colons. (O) Total tumor area. (P) Colon length. (Q) Representative H&E (left) and immunofluorescence of Ki67 (green) in colon sections and Ki67 positive index (right). Scale bars: 100 μm. Data are presented as the mean ± SEM. $*P < .05$, $**P < .01$, $***P < .001$.

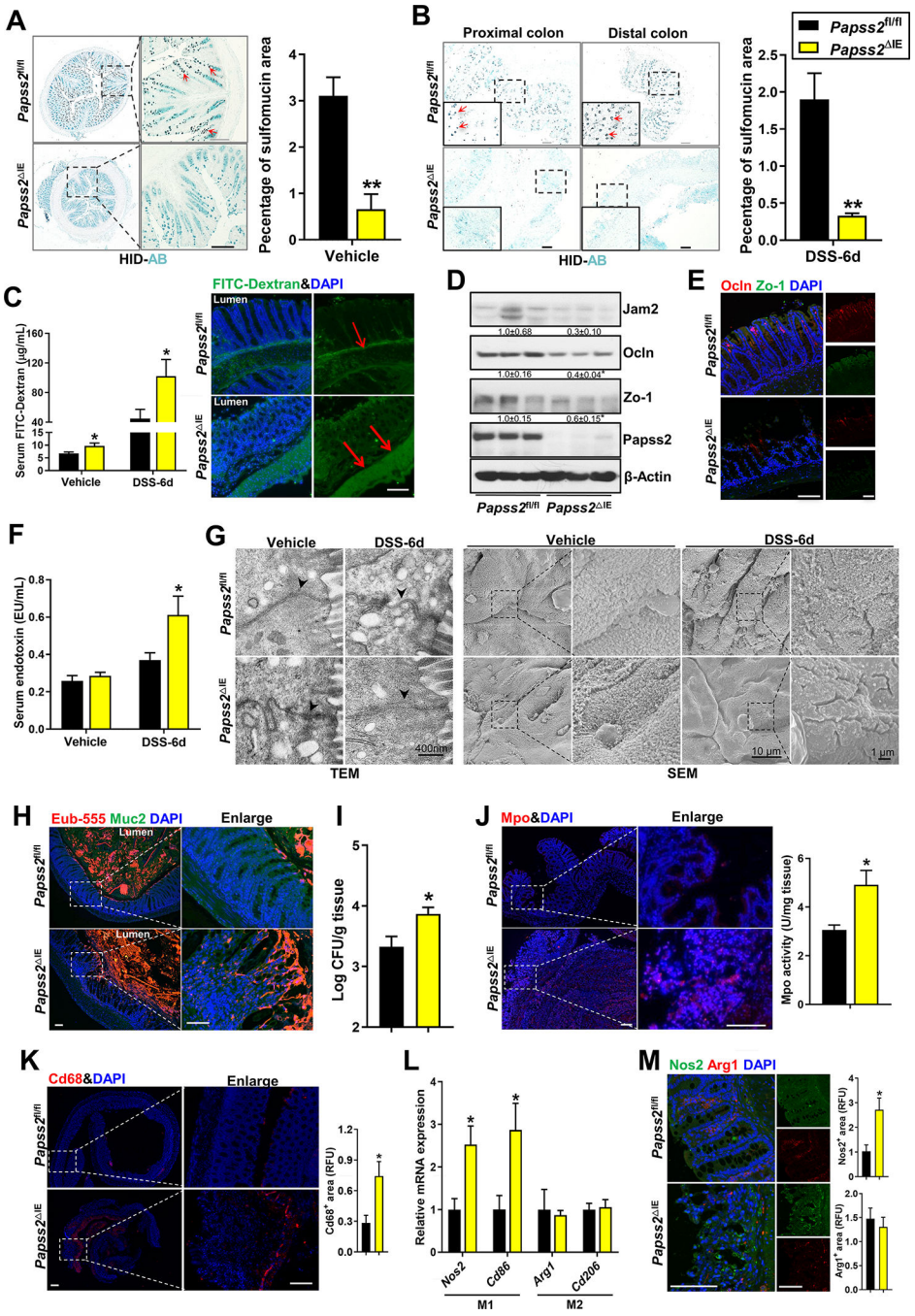

Figure 4. Lack of *Papss2* reduces mucin sulfation and increases intestinal permeability upon colitis challenge.

Mice are the same as described in Figure 2 E–L. (A and B) Representative micrographs and quantifications of HID-AB staining (sulfomucin stains black as indicated by red arrows) in colon sections from mice treated with vehicle (A), or 3% DSS for 6 days (B). Scale bars: 100 μm. (C) Left: serum FITC-dextran. Right: representative micrographs of FITC labeled dextran in colon sections. Red arrows indicate FITC-dextran flow directions. Scale bars: 100 μm. (D and E) Tight junction protein levels were measured by Western blotting (D) and immunofluorescence (E). (F) Serum level of endotoxin. (G) Left: TEM images with

arrowheads indicate tight junctions. Right: SEM images. Scale bars are labeled. (H) Fluorescence *in situ* hybridization (FISH) with Eub-555 probe for bacterial 16S rRNA (red) and immunofluorescence of Muc-2 (green) in Carnoy's fixed paraffin-embedded colonic tissue with contents. Scale bars: 100 μm. (I) Colony Formation Unit (CFU) that measures bacterial translocation to the mesenteric lymph nodes. (J) Immunofluorescence of colonic MPO (red). Shown on the right is the measurement of MPO activity. Scale bars: 100 μm. (K) Immunofluorescence and quantification of Cd68 (red) staining. Scale bars: 100 μm. (L) Relative colonic mRNA levels of M1 and M2 macrophage marker genes. (M) Immunofluorescence and quantifications of Nos2 (greed) and Arg1 (red) signals. Scale bars: 100 μm. n=4–6/group. Data are presented as the mean ± SEM. $*P < .05$, $**P < .01$.

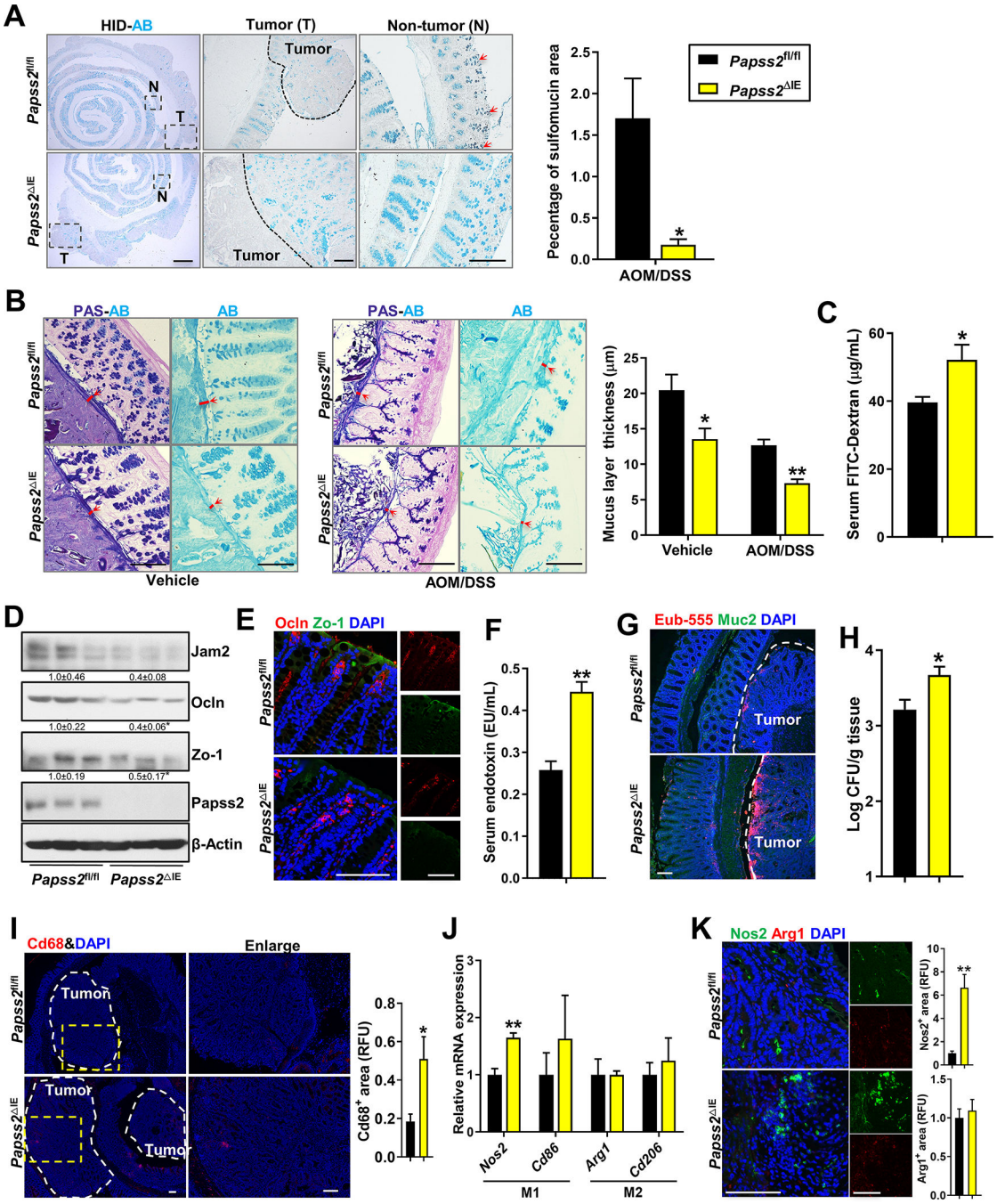

Figure 5. Intestinal ablation of *Papss2* impairs intestinal barrier function and worsens tumor microenvironment in tumor-bearing mice.

Mice are the same as described in Figure 3A–M. (A) Representative micrographs and quantification of HID-AB staining (sulfomucin stains black as indicated by red arrows) in the tumor (T) or non-tumor (N) regions of the *Papss2*$^{fl/fl}$ and *Papss2*$^{\Delta IE}$ mice (n=6). Left scale bars: 1mm; middle and right scale bars: 100 μm. (B) Representative micrographs of PAS-AB and AB staining and quantifications of mucus thickness (thick red lines as indicated by red arrows) in colon sections with contents from vehicle- and AOM/DSS-treated mice. Scale bars: 100 μm. (C) Intestinal permeability measured by serum FITC-

dextran. (D and E) Tight junction protein levels were measured by Western blotting (D) and immunofluorescence (E). (F) Serum level of endotoxin. (G) FISH with Eub-555 probe for bacterial 16S rRNA (red) and immunofluorescence for Muc-2 (green) in Carnoy's fixed paraffin-embedded colon tissue. Scale bars: 100 μm.
(H) Colony Formation Unit (CFU) that measures bacterial translocation to the mesenteric lymph nodes. (I) Immunofluorescence and quantifications of Cd68 (red) in the colon. Scale bars: 100 μm. (J) Relative colonic mRNA levels of M1 and M2 macrophage marker genes. (K) Immunofluorescence and quantifications of Nos2 (greed) and Arg1 (red) signals. Scale bars: 100 μm. n=4–6/group. Data are presented as the mean ± SEM. *$P < .05$, **$P < .01$.

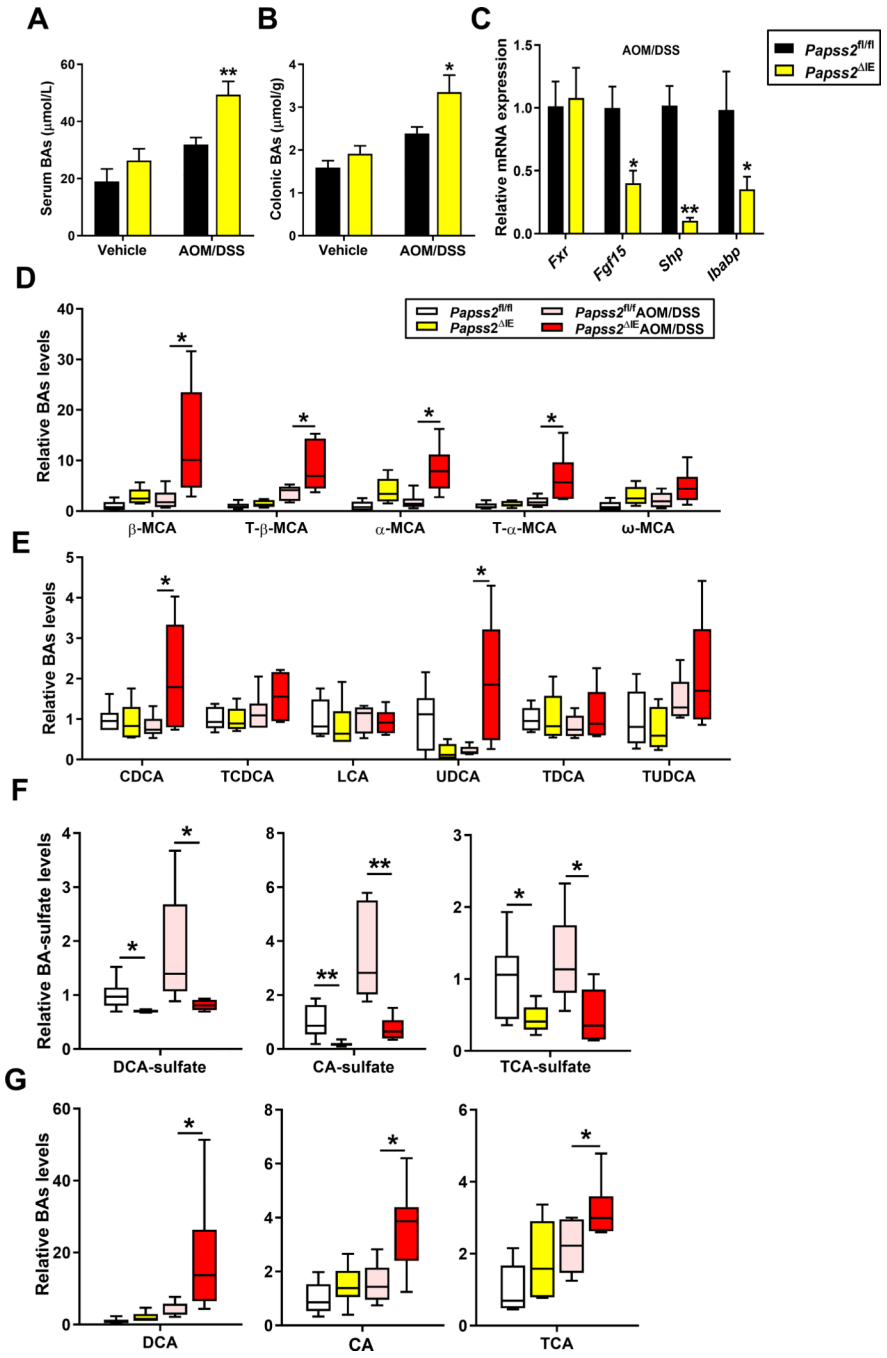

Figure 6. Increased colonic carcinogenesis in *Papss2*$^{\Delta IE}$ mice is accompanied by disruption of bile acid homeostasis and FXR signaling.

Mice are the same as described in Figure 3A–M. (A) Serum bile acids (BAs) levels. (B) Colonic BAs levels. (C) Relative expression of FXR target genes in the colon. (D-G) Relative MCAs levels (D), individual BAs levels (E), DCA-sulfate, CA-sulfate, TCA-sulfate levels (F), and parent DCA, CA, TCA levels (G) in the colon measured by UPLC–QTOFMS. n=4–6/per group. Data are presented as the mean ± SEM. **P* < .05, ***P* < .01.

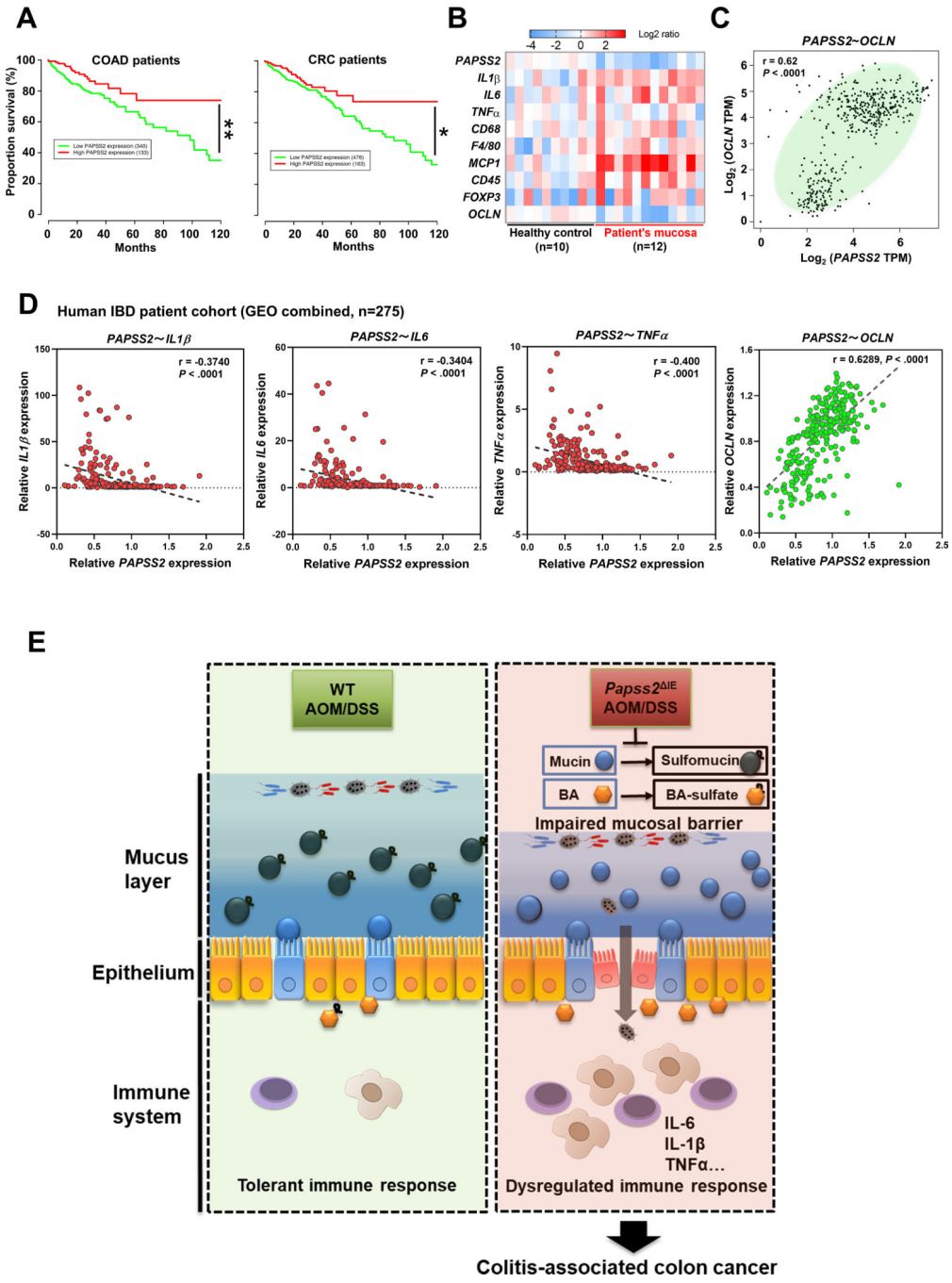

Figure 7. Decreased expression of PAPSS2 correlates with poor clinical outcome of colon cancer patients.

(A) Parsing of human colon adenocarcinoma (COAD) and colorectal cancer (CRC) patient survival curves based on the *PAPSS2* expression. (B) Heatmap comparing gene signatures in colonic mucosa of healthy controls and colon cancer patients (GSE4107). (C) Correlation between the expression of *PAPSS2* and *OCLN* in human COAD patient cohorts from TCGA using GEPIA analyses. (D) Correlations between the expression of *PAPSS2* and *IL-1β*, *IL-6*, *TNFα*, and *OCLN* in human patient cohorts (GSE16879 and GSE11223, n=275). (E)

Schematic model depicting the functions of intestinal PAPSS2 in colitis-associated colon cancer. *$P < .05$, **$P < .01$.